Three-dimensional phase-kink state in a thick stack of Josephson junctions and terahertz radiation

Xiao Hu[1,2,3] and Shizeng Lin[1,2]

[1]*WPI Center for Materials Nanoarchitectonics, National Institute for Materials Science, Tsukuba 305-0047, Japan*

[2]*Graduate School of Pure and Applied Sciences, University of Tsukuba, Tsukuba 305-8571, Japan*

[3]*Japan Science and Technology Agency, 4-1-8 Honcho, Kawaguchi, Saitama 332-0012, Japan*

(Received 5 July 2008; published 9 October 2008)

The dynamics of superconductivity phase in thick stack of Josephson junctions with strong inductive coupling, such as the one realized in layered high-T_c cuprates and possibly the recently discovered FeAs-based superconductors, is investigated under a c-axis bias voltage and in the absence of an external magnetic field. The kink state found previously by the present authors is extended to three dimensions for both rectangular and cylindrical geometries. The IV characteristics are calculated and the distributions of electromagnetic field inside the samples are clarified. The solution for a cylindrical mesa exhibits a higher resonating frequency than that of a square mesa with the same linear size by a factor of ~ 2.4. More importantly, from the radius dependence of the resonance frequency for the cylinder geometry it is possible to confirm directly the kink state and thus to reveal the mechanism of the strong radiation discovered in recent experiments.

DOI: 10.1103/PhysRevB.78.134510 PACS number(s): 74.50.+r, 74.25.Gz, 85.25.Cp

I. INTRODUCTION

Stimulated by the recent progress in radiation of terahertz (THz) electromagnetic waves using a mesa of $Bi_2Sr_2CaCu_2O_{8+\delta}$ (BSCCO) single crystal,[1,2] we investigated the dynamics of superconductivity phase of the intrinsic Josephson junctions with strong inductive couplings. A new dynamics state was found in the absence of an external magnetic field, in which the gauge-invariant phase difference in each junction is characterized by static $\pm\pi$ phase kinks stacked periodically along the c axis, in addition to a phase term evolving linearly with time according to the ac Josephson relation and the plasma term.[3,4] The phase kink permits pumping large dc energy into the plasma oscillation via the ac Josephson effect and enhances strong radiations of THz electromagnetic waves. This state is the only one known so far which counts for the following important features of the coherent radiations observed in Refs. 1 and 2: (1) the frequency is determined by the cavity mode of the mesa sample, (2) the frequency and voltage satisfy the ac Josephson relation, and (3) the radiation takes place in a sharp regime of voltage.

For simplicity, a two-dimensional (2D) solution was worked out explicitly, presuming a state uniform along the in-plane direction of the long edge of the mesa.[3] This solution corresponds to the (1,0) cavity mode. In the present work, we show that the kink state can be extended to three-dimensional (3D), where the phase kink runs in the ab planes and the solution is labeled by the (1,1) cavity mode. The kink state can also exist in samples of the cylinder geometry.

We first derive a set of equations for the shape of the phase kink, the amplitude, and the phase shift of plasma oscillation. An approximate solution can be obtained easily in the strong inductive-coupling limit where the phase kink renders a step function. This formalism releases one from a full computer simulation and can be extended from 2D to 3D straightforwardly.

The present paper is organized as follows. In Sec. II, we formulate the kink state for the (1,0) cavity mode (thus 2D) in a rectangular mesa presented in Ref. 3. The analysis is then extended to 3D in Sec. III and the (1,1) cavity mode is analyzed. The current-voltage curve of the kink state is presented, and the distribution of electromagnetic field is derived. Section IV is devoted to analysis for the cylinder geometry. Radiation of THz electromagnetic waves is addressed under a boundary condition of an effective impedance in Sec. V. Discussions are given in Sec. VI before a brief summary.

II. ONE-DIMENSIONAL KINK IN RECTANGULAR MESA

The coupled sine-Gordon equations for a stack of Josephson junctions[5–7] take the following form when the inductive coupling ζ is large:

$$(\partial_x^2 + \partial_y^2)P_l = (1 - \zeta\Delta^{(2)})(\sin P_l + \beta\partial_t P_l + \partial_t^2 P_l - J_{\text{ext}}), \quad (1)$$

where P_l is the total gauge-invariant phase difference of the lth junction, the lateral directions are scaled by λ_c, time by the plasma frequency ω_p, external current by the critical Josephson current J_c, $\zeta \equiv \lambda_{ab}^2/sD$, $\beta \equiv 4\pi\sigma_c\lambda_c/c\sqrt{\varepsilon_c}$, and $\Delta^{(2)}Q_l = Q_{l+1} + Q_{l-1} - 2Q_l$, with λ_{ab} and λ_c the penetration depths, s (D) the thickness of the superconducting (insulating) layer, σ_c the c-axis conductance due to quasiparticles, ε_c the dielectric constant, and c the light velocity in vacuum.[3,8] We consider first the system under the boundary condition $\partial_n P_l = 0$ with n the normal to the sample edges.[3,4]

For the kink solution of the (1,0) cavity mode of a rectangular mesa, the phase difference P_l is given by[3]

$$P_l(x,t) = \omega t + A\cos\left(\frac{\pi x}{L_x}\right)\sin(\omega t + \varphi) + f_l P^s(x), \quad (2)$$

where $f_l P^s(x)$ is a kink from 0 to $\pm\pi$ with the center at $x = L_x/2$. The first linear term is in accordance with the ac Josephson relation.

In a state characterized by the phase Eq. (2) with $f_l = (-1)^l$ or $f_l = (-1)^{[l/2]}$, Eq. (1) is decoupled. From the static

parts, the relation of current conservation is derived[3]

$$J_{\rm ext} = \beta\omega - \sin\varphi \int_0^{L_x} \frac{dx}{L_x} J_{-1}(Ag_{10}^r)\cos P^s, \tag{3}$$

where $g_{10}^r = \cos(\pi x/L_x)$ and J_ν is the Bessel function of the first kind. The phase kink $P^s(x)$ is governed by the differential equation

$$\partial_x^2 P^s = q\zeta \cos\varphi J_{-1}(Ag_{10}^r)\sin P^s, \tag{4}$$

with $q=4$ for period-2 and $q=2$ for period-4 solutions and the boundary condition $\partial_x P^s = 0$ at the edges. While this differential equation has to be solved numerically, to a good approximation, the phase kink can be described well by $P^s(x) = \phi(x)/2$ with the soliton solution $\phi(x) = 4\arctan\{\exp[(x - L_x/2)/w]\}$. The width of the phase kink is $w \sim 1/\sqrt{\zeta} \sim 10^{-3}$ for BSCCO, which renders the kink almost a step function.

From terms associated with $\sin(\omega t)$ and $\cos(\omega t)$ when the phase in Eq. (2) is subject to Eq. (1), one obtains

$$\frac{1}{2}A\beta\omega = \sin\varphi \int_0^{L_x} \frac{dx}{L_x} g_{10}^r [J_0(Ag_{10}^r) + J_{-2}(Ag_{10}^r)]\cos P^s, \tag{5}$$

$$\frac{1}{2}A[\omega^2 - (\pi/L_x)^2] = \cos\varphi \int_0^{L_x} \frac{dx}{L_x} g_{10}^r [J_0(Ag_{10}^r) - J_{-2}(Ag_{10}^r)]\cos P^s. \tag{6}$$

With the aids of Eq. (5) and the recursion relation of the Bessel functions $zJ_{\nu-1}(z) + zJ_{\nu+1}(z) = 2\nu J_\nu(z)$, Eq. (3) is simplified as

$$J_{\rm ext} = \beta\omega(1 + A^2/4), \tag{7}$$

where the first term clearly counts for the dc ohmic dissipation and the second term is caused by the ac voltage generated by the plasma oscillation, which modifies the otherwise linear *IV* curve.

The four equations (4)–(7) describe the kink state specified by five quantities, namely, $J_{\rm ext}$, ω (i.e., voltage), A, φ, and $P^s(x)$. Especially, the *IV* characteristics can be derived by sweeping the voltage ω.

As the frequency, or equivalently the voltage, approaches the cavity mode $\omega = \pi/L_x$, large plasma oscillations are stimulated and a large external current is shunted by the Josephson current. Just at the cavity frequency Eq. (6) is reduced to

$$\frac{1}{L_x}\int_0^{L_x} dx g_{10}^r [J_0(Ag_{10}^r) - J_{-2}(Ag_{10}^r)]\cos P^s = 0. \tag{8}$$

In the limit of strong inductive coupling, where the phase kink is well approximated by a step function, Eq. (8) is easily solved to yield $A = 2.331$, and then $\sin\varphi = 0.4625$ and $J_{\rm ext} - \beta\omega = 0.2133$ for $\beta = 0.02$ and $L_x = 0.4$ in units of $\lambda_c = 200$ μm, typical for the BSCCO single crystal used in recent experiments.

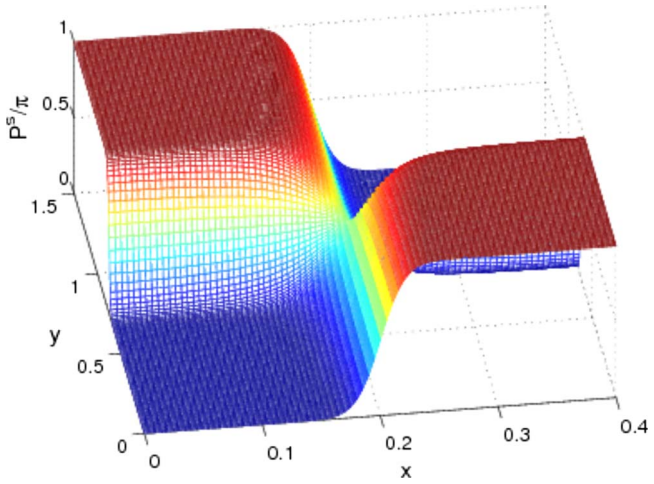

FIG. 1. (Color online) 2D phase kink for the (1,1) cavity mode of a rectangular mesa obtained by numerical integration on Eq. (10).

For comparison, simulations gave $J_{\rm ext} - \beta\omega = 0.37$.[3] Therefore, the present simplified equations give a semiquantitative evaluation for the kink state at the cavity modes.

III. 2D KINK IN RECTANGULAR MESA

Now we look for the state of static phase kink of two lateral dimensions, which corresponds to the (1,1) cavity mode of a rectangular sample

$$P_l(x,y,t) = \omega t + A\cos\left(\frac{\pi x}{L_x}\right)\cos\left(\frac{\pi y}{L_y}\right)\sin(\omega t + \varphi) + f_l P^s(x,y). \tag{9}$$

The equation for the 2D kink is

$$(\partial_x^2 + \partial_y^2)P^s = q\zeta\cos\varphi J_{-1}(Ag_{11}^r)\sin P^s, \tag{10}$$

where $g_{11}^r = \cos(\pi x/L_x)\cos(\pi y/L_y)$ with $\partial_n P^s = 0$ at edges where n is the normal of the edges. The solution obtained by numerical integration is depicted in Fig. 1, with $L_x = 0.4$ and $L_y = 1.5$ as in experiments,[1] and all the prefactors are included into the width of the kink.

The remaining three equations are given by

$$\frac{1}{4}A\beta\omega = \sin\varphi \int_0^{L_x}\int_0^{L_y} \frac{dxdy}{L_xL_y} g_{11}^r [J_0(Ag_{11}^r) + J_{-2}(Ag_{11}^r)]\cos P^s, \tag{11}$$

$$\frac{1}{4}A\left[\omega^2 - \left(\frac{\pi}{L_x}\right)^2 - \left(\frac{\pi}{L_y}\right)^2\right] = \cos\varphi \int_0^{L_x}\int_0^{L_y} \frac{dxdy}{L_xL_y} g_{11}^r [J_0(Ag_{11}^r) - J_{-2}(Ag_{11}^r)]\cos P^s, \tag{12}$$

$$J_{\rm ext} = \beta\omega(1 + A^2/8). \tag{13}$$

Approximating $\cos P^s$ by the 2D step function (see Fig. 1), the *IV* curve is evaluated and displayed in Fig. 2. An

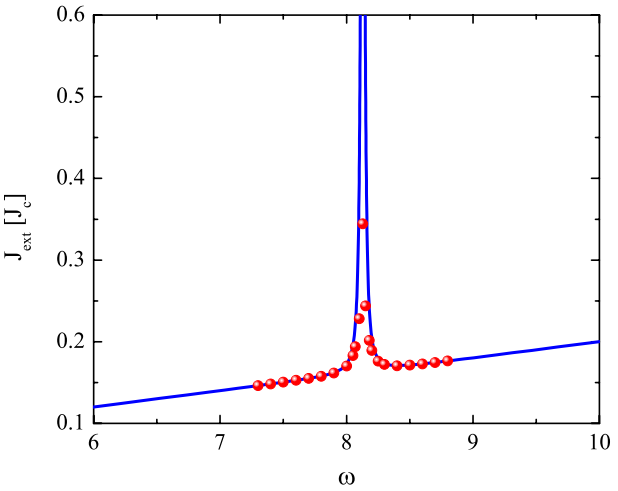

FIG. 2. (Color online) *IV* curves derived by Eqs. (11)–(13) presuming a step-function phase kink (red symbols) and by Eq. (14) (blue lines) for the (1,1) mode of a rectangular mesa with $L_x=0.4$ and $L_y=1.5$. The cavity frequency is $\omega=8.128$, which corresponds to 0.62 THz approximately.

enhancement of the input current appears when the voltage approaches the cavity mode value $\omega=\sqrt{(\pi/L_x)^2+(\pi/L_y)^2}$, where the extra energy is pumped into plasma oscillation.

The way of the system evolving into the resonance state from the linear ohmic regime can be seen more transparently by neglecting A in the right-hand side of Eqs. (11) and (12). One then finds

$$J_{\rm ext}=\beta\omega\left\{1+\frac{2(I_{11}^r)^2}{[\omega^2-(\pi/L_x)^2-(\pi/L_y)^2]^2+(\beta\omega)^2}\right\}, \tag{14}$$

with $I_{11}^r=(1/L_xL_y)\int_0^{L_x}\int_0^{L_y}dxdyg_{11}^r\cos P^s$. A similar expression has been derived for the one-dimensional (1D) kink state.[4] The development of the resonance is captured analytically by the above expression, although it becomes invalid around the resonating regime where A is not small any more. In the strong inductive-coupling limit where the phase kink takes a step function, $I_{11}^r=4/\pi^2$.

As seen in Fig. 2, the two treatments give the same *IV* curves outside the resonance regime where the plasma amplitude is small. Usage of Eqs. (11) and (12) improves the description of the resonating state over Eq. (14).

The ac electromagnetic fields are given by $E^z(x,y)=\partial_t\tilde{P}(x,y)$, $B^x(x,y)=-\partial_y\tilde{P}(x,y)$, and $B^y(x,y)=\partial_x\tilde{P}(x,y)$, with $\tilde{P}(x,y)$ the plasma term in Eq. (9).[3] As shown in Fig. 3, the electric field takes the maximal absolute value at the four corners, whereas the magnetic field is maximal at the centers of the edges. The magnetic field penetrates into the system from the two edges along the x direction, flows away from the two edges along the y direction, and the pattern oscillates with time by switching x and y. The y component of magnetic field is larger in absolute value than the x component since the system is longer in the y direction. Both the electric and magnetic fields are shielded in the superconducting sample and thus the central part of the mesa is free of electromagnetic fields. As discussed in Ref. 3, in the resonance state at cavity modes higher harmonics exist and the simple symmetry in Fig. 3 is modified.

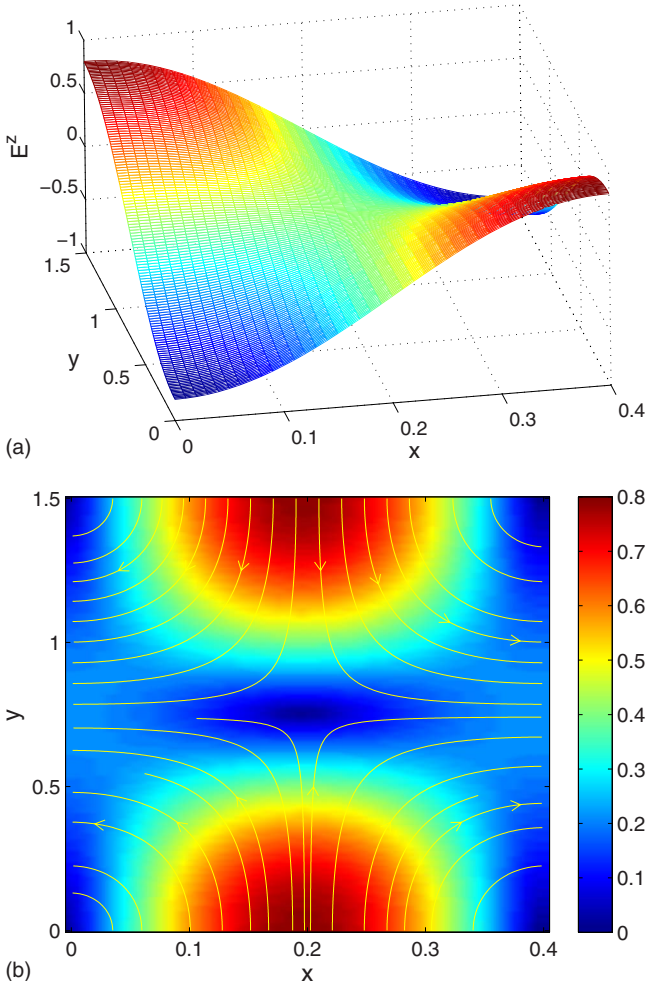

FIG. 3. (Color online) Distribution of (a) ac electric field and (b) ac magnetic field in for the (1,1) cavity mode of the rectangular mesa.

The static phase kink generates static Josephson currents in junctions as depicted in Fig. 4. The patterns with swapped upward and downward Josephson currents are stacked periodically along the c axis according to $f_l=(-1)^l$ or $f_l=(-1)^{[l/2]}$.

IV. KINK STATE IN CYLINDER GEOMETRY

Now we consider a sample of cylindrical shape and radius a. For the (0,1) mode in the cylinder geometry which is isotropic azimuthally, the total phase difference is given by

$$P_l(\rho,t)=\omega t+AJ_0\left(\frac{v_{01}\rho}{a}\right)\sin(\omega t+\varphi)+f_lP^s(\rho), \tag{15}$$

where $v_{01}=3.8317$ is the first zero of J_1.

The equation for the static phase kink in cylinder is

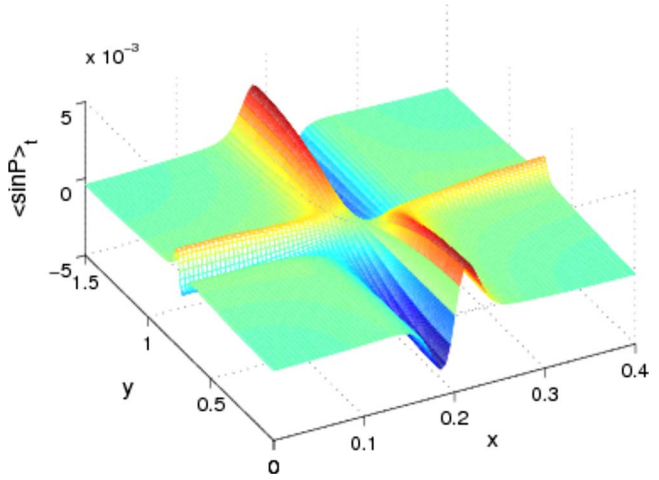

FIG. 4. (Color online) Distribution of static Josephson current for the (1,1) cavity mode of a rectangular mesa.

$$[\partial_\rho^2 + (1/\rho)\partial_\rho]P^s = q\zeta \cos\varphi J_{-1}(Ag_{01}^c)\sin P^s, \tag{16}$$

with $g_{01}^c = J_0(v_{01}\rho/a)$ under the boundary condition $\partial_\rho P^s = 0$ at the edge. The solution obtained by numerical integration is displayed in Fig. 5 for $a=0.4$. The phase crosses $\pi/2$ at $\rho = u_{01}a/v_{01}$, where $u_{01}=2.4048$ is the first zero of J_0.

The remaining equations are given by

$$\frac{1}{2}A\beta\omega J_0^2(v_{01}) = \sin\varphi \int_0^a \frac{\rho d\rho}{a^2} g_{01}^c [J_0(Ag_{01}^c) + J_{-2}(Ag_{01}^c)]\cos P^s, \tag{17}$$

$$\frac{1}{2}A[\omega^2 - (v_{01}/a)^2]J_0^2(v_{01}) = \cos\varphi \int_0^a \frac{\rho d\rho}{a^2} g_{01}^c [J_0(Ag_{01}^c) - J_{-2}(Ag_{01}^c)]\cos P^s, \tag{18}$$

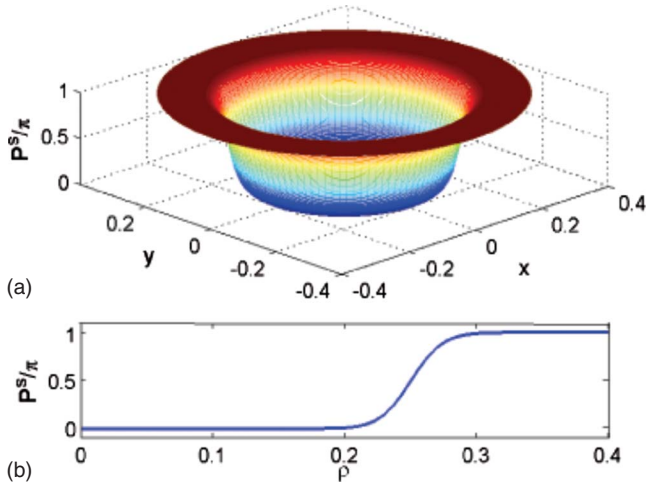

FIG. 5. (Color online) (a) Phase kink and (b) radial dependence of phase in a cylinder sample obtained by numerical integration on Eq. (16).

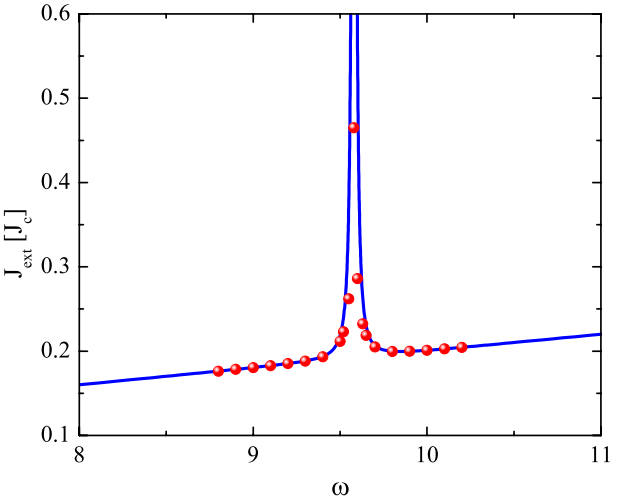

FIG. 6. (Color online) *IV* curves derived by Eqs. (17)–(19) presuming a step-function phase kink (red symbols) and by Eq. (20) (blue lines) for the (0,1) mode of a cylinder sample of $a=0.4$. The cavity frequency is $\omega=9.579$, which corresponds to 0.73 THz approximately.

$$J_{\text{ext}} = \beta\omega[1 + A^2 J_0^2(v_{01})/2], \tag{19}$$

where $J_0(v_{01}) = -0.4028$ and the normalization relation $\int_0^a J_0^2(v_{01}\rho/a)\rho d\rho = a^2 J_0^2(v_{01})/2$ has been used. The frequency of the (0,1) cavity mode for the cylinder geometry is $\omega = v_{01}/a$ which reaches 1 THz when $a = 58.5$ μm.

The *IV* curve is displayed in Fig. 6, taking $\cos P^s$ as the step function. For comparison we also show the *IV* curve evaluated by the following expression:

$$J_{\text{ext}} = \beta\omega\left\{1 + \frac{2(I_{01}^c)^2/J_0^2(v_{01})}{[\omega^2 - (v_{01}/a)^2]^2 + (\beta\omega)^2}\right\}, \tag{20}$$

with $I_{01}^c = (1/a^2)\int_0^a \rho d\rho g_{01}^c \cos P^s$ obtained in the same way as Eq. (14). For the step-function phase kink, $I_{01}^c = 0.1701$. Once again the two evaluations agree with each other outside the resonance regime.

The ac electromagnetic fields take the following forms: $E^z = A\omega J_0(v_{01}\rho/a)$, $B^x = A(v_{01}y/2\rho a)J_1(v_{01}\rho/a)$, and $B^y = -A(v_{01}x/2\rho a)J_1(v_{01}\rho/a)$. The distribution of electromagnetic field is shown in Fig. 7 which oscillates with time. The electric field takes the maximum at the center of cylinder, changes its sign at $\rho = u_{01}a/v_{01} = 0.6276a$, and at the perimeter it reaches −0.4028 of the maximum value [Figs. 7(a) and 7(b)]. The magnetic field is circular; the amplitude is zero at both the center and edge of the cylinder, and presumes its maximum at $\sim a/2$ [Figs. 7(c) and 7(d)]. The distribution of the static Josephson current generated by the static phase kink is displayed in Fig. 8. The patterns with swapped upward and downward Josephson currents are stacked periodically in the c axis.

V. RADIATION OF ENERGY

The boundary condition of a single junction subject to radiation was discussed in literatures.[9–11] There is a significant mismatch of the impedance between the junctions and

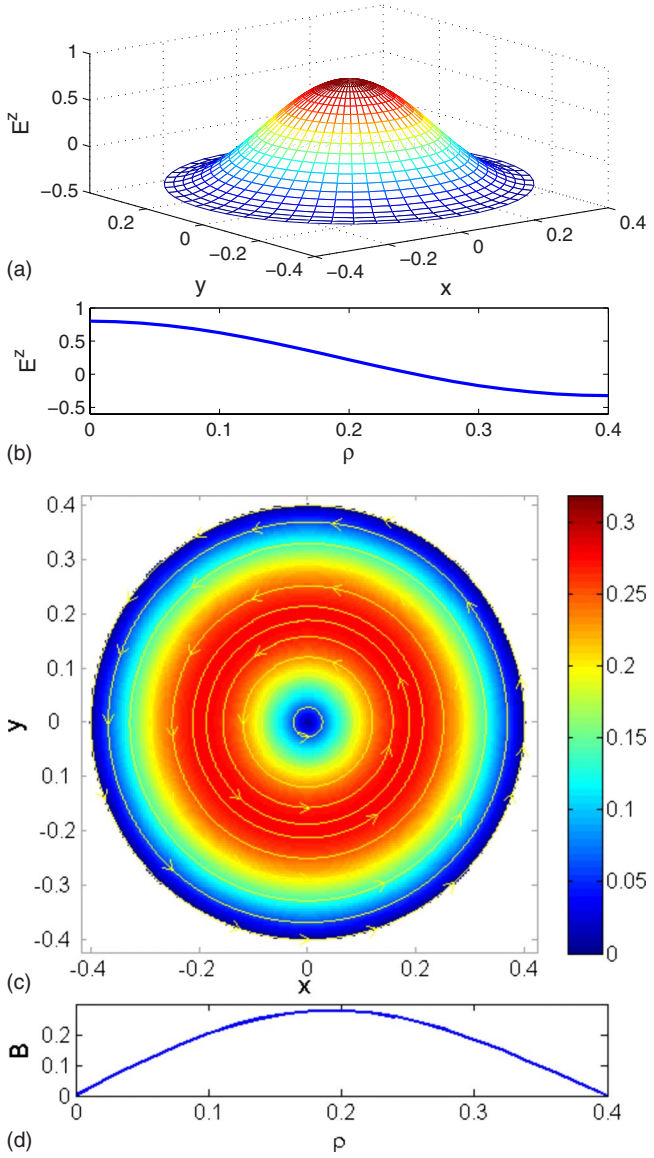

FIG. 7. (Color online) Distribution of ac electric field [(a) and (b)] and magnetic field [(c) and (d)] in a cylinder sample.

outside space. As in the previous work,[3] we model the space by an effective impedance Z. The effective impedance should be very large due to the small thickness of the sample compared with λ_c.[12] We have confirmed that the cavity resonance based on the kink state is stable for $|Z| > 50$.

The *IV* characteristics should be modified when the radiation is present. Since the radiation is governed by the attached impedance, the *IV* characteristics can be evaluated simply by an effective parallel circuit. With a simple dimension counting one finds for a real impedance Z (Ref. 13),

$$J_{\rm ext} = \beta\omega + \beta\omega A^2/4 + \omega A^2/(ZL_x), \tag{21}$$

$$J_{\rm ext} = \beta\omega + \beta\omega A^2/8 + \omega A^2(1/L_x + 1/L_y)/(2Z), \tag{22}$$

$$J_{\rm ext} = \beta\omega + \beta\omega A^2 J_0^2(v_{01})/2 + \omega A^2 J_0^2(v_{01})/(Za), \tag{23}$$

for the (1,0) mode uniform in the direction of long edge and the (1,1) mode of the rectangular mesa, and for the (0,1) mode of the cylindrical mesa, respectively. The density of radiation energy measured by the Poynting vector then reads

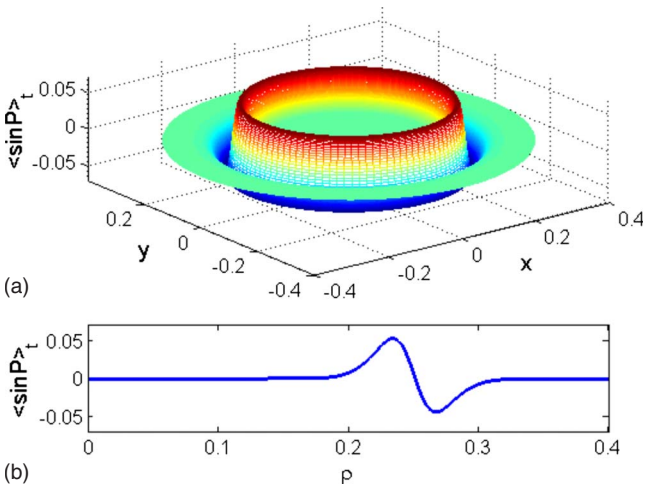

FIG. 8. (Color online) (a) Distribution and (b) radial dependence of Josephson current for the (0,1) mode of a cylinder sample.

$$P_{10}^r = \omega^2 A^2/(2Z), \tag{24}$$

$$P_{11}^r = \omega^2 A^2/(4Z), \tag{25}$$

$$P_{01}^c = \omega^2 A^2 J_0^2(v_{01})/(2Z), \tag{26}$$

for the respective modes.

Presuming the same impedance, we evaluate the ratio between the Poynting vectors at the corresponding cavity modes when the linear sample size is the same $2a = L(=L_x = L_y)$: $P_{01}^c/P_{10}^r = 3.125$ and $P_{01}^c/P_{11}^r = 1.898$, where the maximal amplitudes $A = 2.331$ for (1,0) mode and 2.991 for (1,1) mode of the rectangular mesa, and 4.194 for (0,1) mode of the cylinder geometry have been used.

There are three factors in determining the Poynting vector: the maximal plasma amplitude, the factor for the electromagnetic field at the edge, and the cavity frequency. In cylinders the electromagnetic fields are isotropic azimuthally and the system can make a full use of the phase kink in pumping dc energy into plasma oscillations, which results in a large plasma amplitude. The (1,1) mode in the rectangular mesa is also better than the (1,0) mode since the former can use a 2D phase kink. While the electric field is maximal at the edges of the rectangular mesa, the edge electric field for the cylinder geometry is only 40% of its maximum taken at the center of the cylinder. This suppresses the radiation power as in Eq. (26). The cavity frequency in the cylindrical geometry is superior to the rectangular geometry by a factor of ~2.4 for the same linear system size.

While the cylinder geometry exhibits a large density of power emission at the sample surface, the energy is radiated uniformly in the azimuthal direction. In applications one needs to focus to a small angle. In contrast, the directivity of the radiation from a rectangular mesa is helpful for gathering energy efficiently.

As can be seen in Eq. (8) and the counterparts for the other modes, the plasma amplitude at the cavity resonance

does not depend on the system size. Therefore, we can increase the radiation energy by adopting smaller samples with larger cavity frequency according to Eqs. (24)–(26).

VI. DISCUSSIONS AND SUMMARY

In the present paper, only the fundamental frequency is kept for the plasma contribution to the total phase difference. This treatment is justified when the system is off resonance, where the amplitude of plasma oscillation is small and higher harmonics can be neglected safely.

We have checked the validity of this treatment at the cavity resonance for the cavity mode (1,0) of the rectangular mesa by comparing the estimates thus obtained with those by accurate simulations which include automatically all orders of higher harmonics.[3] We expect that this approximation also provides reasonable estimates for the (1,1) cavity modes of the rectangular mesa and for the cylinder geometry.

In the resonating regime, the plasma part is much enhanced and higher harmonics appear.[3] The number of equations governing the kink state is $2m+2$ when up to the mth harmonics are covered. Here we provide equations merely including the fundamental frequency with $m=1$. While the formulas can be extended easily to higher harmonics, the resultant equations are much more complex and take heavy numerics to solve. Discussions on this point will be reported elsewhere.[14]

In the kink solution, the spatial part of the plasma term is the eigenfunction of the Laplace operator in the respective geometry with zero (or in presence of radiation very small) normal derivative at the edge, proportional to the magnetic field. In the cylinder geometry, it gives a cavity frequency v_{01}/a with a the radius of cylinder and $v_{01}=3.3817$ the first zero of J_1. For a state presuming zero (or very small) electric field at the boundary, the typical frequency should be u_{01}/a, where $u_{01}=2.4048$ is the first zero of J_0. Therefore, detecting the size dependence of the cavity frequency in the cylinder geometry can tell directly what state is realized inside the system. Since a rectangular mesa will give cavity frequency of π/L for both of the two cases, the cylinder geometry is unique in determining the state realized in the junctions and thus the mechanism of the strong radiation observed recently in experiments.

The present analysis reveals the way how the stack of Josephson junctions convert the dc energy to ac electromagnetic radiation by formulating out explicitly the oscillation amplitude and the frequency. The far-field radiation pattern is determined merely by the spatial part of the plasma term and is the same as a thin capacitor subject to an ac driving voltage. Analyses on far-field radiation patterns for various modes are available in literature,[15] and the results can be compared with those observed for the THz radiations from mesas of BSCCO single crystal. A detailed discussion will also be given in Ref. 14.

To summarize, we have worked out explicitly the kink state in Josephson junctions of strong inductive coupling in 3D for both rectangular and cylindrical geometries. A set of equations are provided which permits one to understand the kink state without heavy numerics. The *IV* characteristics are revealed to be very nonlinear due to the cavity resonance where the plasma oscillation is much enhanced. The solution for a cylindrical mesa provides a higher resonating frequency than that of a square mesa with the same linear size by a factor of ~ 2.4. Investigation on the size dependence of the resonating frequency in the cylinder geometry can give a direct evidence for the state realized in the stack of Josephson junctions and thus can reveal the mechanism of the strong radiation discovered recently. Experiments using cylindrical mesas are highly anticipated.

ACKNOWLEDGMENTS

The authors thank M. Tachiki and K. Kadowaki for discussions. This work was supported by the WPI Initiative on Materials Nanoarchitectonics, MEXT of Japan, and by CREST-JST, and partially by ITSNEM of CAS.

[1] L. Ozyuzer, A. E. Koshelev, C. Kurter, N. Gopalsami, Q. Li, M. Tachiki, K. Kadowaki, T. Yamamoto, H. Minami, H. Yamaguchi, T. Tachiki, K. E. Gray, W. K. Kwok, and U. Welp, Science **318**, 1291 (2007).

[2] K. Kadowaki, H. Yamaguchi, K. Kawamata, T. Yamamoto, H. Minami, I. Kakeya, U. Welp, L. Ozyuzer, A. Koshelev, C. Kurter, K. E. Gray, and W.-K. Kwok, Physica C **468**, 634 (2008).

[3] S. Z. Lin and X. Hu, Phys. Rev. Lett. **100**, 247006 (2008).

[4] A. E. Koshelev, arXiv:0804.0146 (unpublished).

[5] M. Tachiki, T. Koyama, and S. Takahashi, Phys. Rev. B **50**, 7065 (1994).

[6] S. Sakai, P. Bodin, and N. F. Pedersen, J. Appl. Phys. **73**, 2411 (1993).

[7] R. Kleiner, T. Gaber, and G. Hechtfischer, Phys. Rev. B **62**, 4086 (2000).

[8] S. Lin, Xiao Hu, and M. Tachiki, Phys. Rev. B **77**, 014507 (2008).

[9] D. N. Langenberg, D. J. Scalapino, B. N. Taylor, and R. E. Eck, Phys. Rev. Lett. **15**, 294 (1965).

[10] L. N. Bulaevskii and A. E. Koshelev, Phys. Rev. Lett. **97**, 267001 (2006).

[11] L. N. Bulaevskii and A. E. Koshelev, J. Supercond. Novel Magn. **19**, 349 (2006).

[12] A. E. Koshelev and L. N. Bulaevskii, Phys. Rev. B **77**, 014530 (2008).

[13] A better treatment is possible and will be reported elsewhere.

[14] S. Z. Lin and X. Hu, arXiv:0809.5169 (unpublished).

[15] M. Leone, IEEE Trans. Electromagn. Compat. **45**, 486 (2003).